https://doi.org/10.5194/egusphere-2023-3061
Preprint. Discussion started: 22 January 2024

Quasi Real-Time Tsunami Early Warning Assessment Based on Finite Fault models

Matías Sifón[1], Mauricio Fuentes[2], Sebastian Riquelme[3], Rodrigo Sánchez[3], Sebastian Arriola[3]

[1]Department of Oceanography, Hydrographic and Oceanographic Service of the Chilean Navy, Valparaíso, 2360007, Chile
[2]Department of Geophysics, University of Chile, Santiago, 8370449, Chile
[3]Seismological National Center, University of Chile, Santiago, 8370449, Chile

Correspondence to: Matias Sifon (matias.sifon@ug.uchile.cl)

Abstract. In Chile, Tsunami Early Warning relies on a precomputed set of scenarios for places near the tsunami generation zone. These scenarios are non-realistic and are computed from a uniform constant slip over the rupture surface, because of the short reaction time for the local authorities to manage the threat. Here, we present a new methodology that allows quasi-real time tsunami modelling using a finite fault model inversion to evaluate tsunami threat levels. A linear approximation at first order terms of the shallow water wave equations turns into a numerical solver that can be implemented on a programming language. As a case of study, the proposed method is applied in Chile. The results show that it is possible to obtain realistic threat levels and arrival times for the tsunami in progress. Once the finite fault is calculated, it takes a minute to produce the warning maps.

The proposal considers realistic heterogeneous and kinematic fault models of seismic sources obtained rapidly using continuous GPS, strong motion and broadband records, expanding the evaluation capabilities of Tsunami Early Warning Systems. Using directly the finite fault avoids the unrealistic model of uniform slip distribution and diminishes the uncertainty imposed by precomputed scenarios.

1 Introduction

Chile is one of the most highly active seismic countries in the world (Madariaga, 1998). In the XX century Chile has hosted 5 tsunamis generated by large earthquakes: Valparaíso 1906, Atacama 1922, Valdivia 1960, Valparaiso 1985, Antofagasta 1995. This list includes the largest earthquake instrumentally recorded. The 1960 Mw 9.5 Valdivia Earthquake (Kanamori, 1977; Barrientos y Ward, 1990; Stein y Michael, 2003; Lomnitz, 2004). Therefore, the Chilean case is especially sensitive. Also, the short distance between the subduction interface (where most tsunamis are triggered) and the coast make near field tsunamis to arrive faster than other countries. This results in a very short reaction time due to the location earthquake hypocenter (Fritz et al., 2011; Catalán et al., 2015; Aránguiz et al., 2015; Fuentes et al., 2017, Catalan et al., 2020).

To mitigate disaster risk, tsunami warning in Chile relies on a precomputed set of earthquake scenarios with uniform slip distribution. Once the magnitude and location are determined, the system chooses the source and the tsunami from the database

https://doi.org/10.5194/egusphere-2023-3061
Preprint. Discussion started: 22 January 2024

following some criteria (Catalan et al., 2020). This strategy avoids the use of on the fly modelling that would normally take several hours. Instead, it evaluates the tsunami threat in very short times, becoming a feasible alternative to give enough time to the Chilean Emergency Response Office to handle the threat. However, there are many limitations using this method: First, the earthquake is not realistic. Seismic sources in the near field must be modelled including variable slip. Second, the system always assumes a subduction type earthquake. Nowadays, this strategy is recommended by UNESCO/IOC especially for countries that cannot wait for a threat message issued by a tsunami monitoring agency like the Pacific Tsunami Warning Center (PTWC) or a tsunami model in the near field due to the short time between the generation and arrival to coasts (UNESCO/IOC, 2017).

The difference in slip distribution between the precomputed scenario with uniform slip and the rupture process, underestimates the tsunami runup (Geist, 2002; Ruiz et al., 2015; Fuentes et al., 2019) up to 6 times. Therefore, it is necessary to incorporate new strategies to accurately assess threats for the authorities.

Fuentes et al (2019) proposes a numerical solver that solves the linear water wave equations. The methodology can be incorporated in real time because it solves the problems mentioned above.

This paper presents a methodology that uses the Finite Fault Model as input for an improved numerical model proposed by Fuentes et al. (2019) to obtain a tsunami threat asset that could be used in real time.

2 Methodology

2.1 Numerical Tsunami Modelling

To obtain the fastest possible solution, we employ the Non-Homogeneous Linear Shallow Water Equation (Eq 1):

$$\begin{aligned} &\eta_{tt} - g((h\eta_x)_x + (h\eta_y)_y) = \zeta_{tt}\ , \\ &\eta(x,y,0) = \zeta_0\,(x,y) \\ &\eta_t(x,y,0) = 0 \end{aligned} \tag{1}$$

Where $\zeta_0\,(x,y)$ is the initial condition and $\zeta(x,y,0)$ is the Inhomogeneous forcing term.

To numerically solve it, a collocated grid is used in a finite difference scheme. The domain is discretized as $(x_i, y_j) = (i\Delta x, j\Delta y)\,, i = 0,\dots,n_x; j = 0,\dots,m_y$ and $t_k = k\Delta t$ represent the increments in space (x,y) and time, respectively. For simplicity, it is commonly adopted to set $\Delta x = \Delta y =: \Delta s$. Then, variables are discretized as $\eta(x_i, y_j, t_k) = \eta_{i,j}^k$

The iterative expression to obtain the water surface is given by Eq. 2.

$$\eta_{i,j}^{k+1} = \left[2 - R\left(h_{i+\frac{1}{2},j} + h_{i,j+\frac{1}{2}} + h_{i-\frac{1}{2},j} + h_{i,j-\frac{1}{2}}\right)\right]\eta_{i,j}^k - \eta_{i,j}^{k-1} + \tag{2}$$

$$Rh_{i+\frac{1}{2},j}\eta_{i+1,j}^k + Rh_{i-\frac{1}{2},j}\eta_{i-1,j}^k + Rh_{i,j+\frac{1}{2}}\eta_{i,j+1}^k + Rh_{i,j-\frac{1}{2}}\eta_{i,j-1}^k + \zeta_{i,j}^{k+1} - 2\zeta_{i,j}^k + \zeta_{i,j}^{k-1}$$

where $R = g\left(\frac{\Delta t}{\Delta s}\right)^2$. Intermediate points are estimated by means of linear interpolation $p_{i\pm\frac{1}{2}} = \frac{p_i + p_{i\pm1}}{2}$.

https://doi.org/10.5194/egusphere-2023-3061
Preprint. Discussion started: 22 January 2024

2.2 Initial Condition

The tsunami is initiated by an underwater perturbation. Depending on the size and duration of this disturbance, time can be neglected, and a static case should be preferred. Otherwise, when temporal aspects of the source, such as duration, rupture velocity, and source time energy release, cannot be ignored, they need to be included in the equations (Riquelme and Fuentes, 2021).

2.2 Static Case

When no forcing term is required ($\zeta = 0$), the tsunami modeling can be posed as a static generation, by translating the underwater perturbation as a water initial disturbance. Since no initial velocity is introduced, the first terms in Eq. (2) are given by Eq. (3).

$$\eta^0_{i,j} = \zeta_{0\,i,j} \tag{3}$$

$$\eta^1_{i,j} = \left[1 - \frac{R}{2}\left(h_{i+\frac{1}{2},j} + h_{i,j+\frac{1}{2}} + h_{i-\frac{1}{2},j} + h_{i,j-\frac{1}{2}}\right)\right]\zeta_{0\,i,j} + \frac{R}{2}\left(h_{i+\frac{1}{2},j}\zeta_{0\,i+1,j} + h_{i-\frac{1}{2},j}\zeta_{0\,i-1,j} + h_{i,j+\frac{1}{2}}\zeta_{0\,i,j+1} + h_{i,j-\frac{1}{2}}\zeta_{0\,i,j-1}\right)$$

The term $\eta^1_{i,j}$ is obtained by imposing that $\eta^{-1}_{i,j} = \eta^1_{i,j}$ (null time derivative/velocity condition), inserting in Eq. (2) and solving for $\eta^1_{i,j}$.

2.2 Kinematic Case

If the time history of the source needs to be included, ζ defines the evolution of the perturbation with null initial conditions

$$\eta^0_{i,j} = 0 \tag{4}$$

$$\eta^1_{i,j} = \zeta^1_{i,j} - \zeta^0_{i,j}$$

Again, $\eta^1_{i,j}$ is obtained by imposing that $\eta^{-1}_{i,j} = \eta^1_{i,j}$ and assuming that $\zeta_t(x, y, 0) = 0$ (No vertical velocity before the perturbation).

Then, Eq. (2) is iterated to propagate tsunami waves.

2.3 Boundary conditions

There are two kinds of boundary conditions. First, waves that leave the domain cannot return as reflected waves. This open-boundary condition can be treated in different ways. The second condition requires a full reflection at solid boundaries (coast), which is imposed throughout Neumann boundary conditions.

2.3.1 Open Boundary Condition

At regions where the waves must leave the domain with no interactions to avoid artificial reflections, an open boundary condition is set. There are several techniques to treat this kind of problems, such as Perfect Matching Layer (PML),

https://doi.org/10.5194/egusphere-2023-3061
Preprint. Discussion started: 22 January 2024

characteristic extrapolation (Riemann solver), among others. Here, we select the damping layer method, where an extra layer surrounds the original domain. In this layer, the waves face resistance until they vanish.

The damping rate function is defined as

$$\begin{aligned} \alpha(x,y) &= 0, && (x,y) \in Comp.Domain \\ \alpha(x,y) &= \gamma_1(x), && x \notin Comp.Domain \\ \alpha(x,y) &= \gamma_2(y), && y \notin Comp.Domain \end{aligned} \tag{5}$$

For simplicity, the damping region width around the domain is constant. The γ_i functions must be zero at the domain boundary (continuity) and strictly increasing outward. Here, we use quadratic damping $\gamma_i(\kappa) = C_i\kappa^2$, where κ is the local variable in the damping layer. In order to well-define the α function, it is easier to take $C_1 = C_2$ (see Figure 1a).

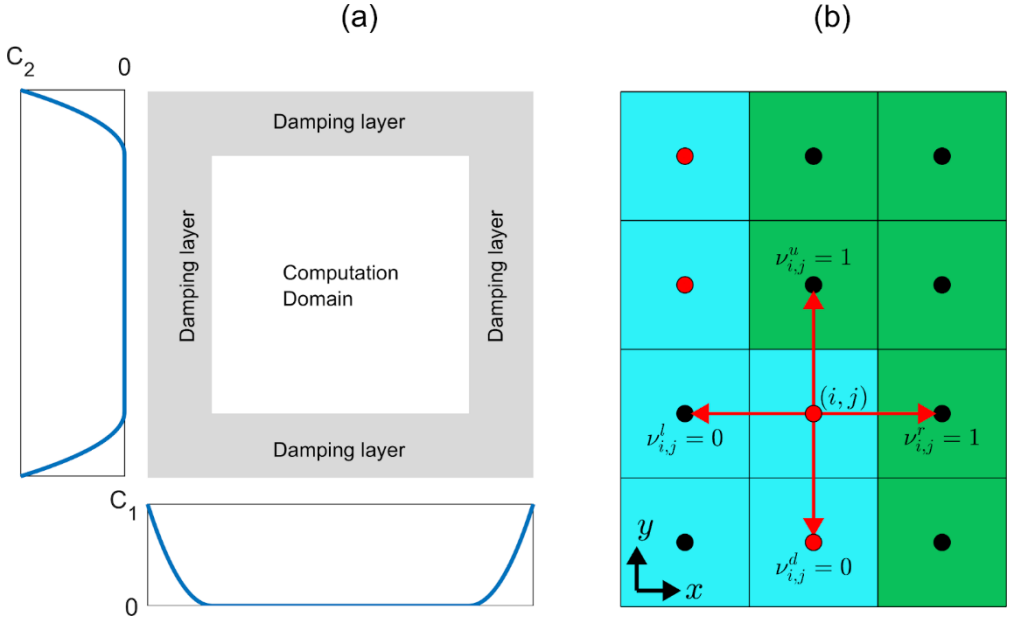

Figure 1: Sketch of the boundary conditions. (a) Damping layer for open boundary conditions. (b) Stencil for Neumann boundary condition. Green cells represent land and sky-blue cells are below the water. Red dots stand for cells in water with active boundary conditions, because at least one of their neighbours are on land.

Then, the reformulated equation to be solved is

$$\eta_{tt} + \alpha\eta_t - g((h\eta_x)_x + (h\eta_y)_y) = \zeta_{tt} \tag{6}$$

and the corresponding numerical solver is

$$\eta_{i,j}^{k+1} = \frac{1}{\left(1 + \frac{\alpha_{i,j}\Delta t}{2}\right)}\{\left[2 - R\left(h_{i+\frac{1}{2},j} + h_{i,j+\frac{1}{2}} + h_{i-\frac{1}{2},j} + h_{i,j-\frac{1}{2}}\right)\right]\eta_{i,j}^k + \left(\frac{\alpha_{i,j}\Delta t}{2} - 1\right)\eta_{i,j}^{k-1} +$$

$$Rh_{i+\frac{1}{2},j}\eta_{i+1,j}^k + Rh_{i-\frac{1}{2},j}\eta_{i-1,j}^k + Rh_{i,j+\frac{1}{2}}\eta_{i,j+1}^k + Rh_{i,j-\frac{1}{2}}\eta_{i,j-1}^k + \zeta_{i,j}^{k+1} - 2\zeta_{i,j}^k + \zeta_{i,j}^{k-1}\} \tag{7}$$

For convenience, we define the following coefficients

https://doi.org/10.5194/egusphere-2023-3061
Preprint. Discussion started: 22 January 2024

$$A_{i,j} = \frac{2}{(\alpha_{i,j}\Delta t + 2)}\left[2 - R\left(h_{i+\frac{1}{2},j} + h_{i,j+\frac{1}{2}} + h_{i-\frac{1}{2},j} + h_{i,j-\frac{1}{2}}\right)\right] \quad (8)$$

$$D_{i,j} = \frac{\alpha_{i,j}\Delta t - 2}{\alpha_{i,j}\Delta t + 2}$$

$$B^r_{i,j} = \frac{2Rh_{i+\frac{1}{2},j}}{\alpha_{i,j}\Delta t + 2}$$

$$B^l_{i,j} = \frac{2Rh_{i-\frac{1}{2},j}}{\alpha_{i,j}\Delta t + 2}$$

$$B^d_{i,j} = \frac{2Rh_{i,j-\frac{1}{2}}}{2 + \alpha_{i,j}\Delta t}$$

$$B^u_{i,j} = \frac{2Rh_{i,j+\frac{1}{2}}}{2 + \alpha_{i,j}\Delta t}$$

Super-indices *r*,*l*,*d* and u stand for *right*, *left*, *down*, *up*. Then, the numerical scheme is

$$\eta^{k+1}_{i,j} = A_{i,j}\eta^k_{i,j} + D_{i,j}\eta^{k-1}_{i,j} + B^r_{i,j}\eta^k_{i+1,j} + B^l_{i,j}\eta^k_{i-1,j} + B^d_{i,j}\eta^k_{i,j+1} + B^u_{i,j}\eta^k_{i,j-1} + \frac{2}{(\alpha_{i,j}\Delta t + 2)}\left(\zeta^{k+1}_{i,j} - 2\zeta^k_{i,j} + \zeta^{k-1}_{i,j}\right) \quad (9)$$

2.3.2 Coastal Boundary Condition

The coastlines represent the frontiers between water and land. In this approach, they act as perfect reflectors. To model this reflection, the Neumann boundary condition is employed

$$\frac{\partial \eta}{\partial \hat{n}} = \nabla\eta \cdot \hat{n} = 0 \quad (10)$$

where $\hat{n}$ represents the unit exterior normal vector. In cartesian coordinates, at each cell, the condition simplifies as

$$\eta_x = 0, \ \ if \ \ \hat{n} = \pm\hat{\imath} \ \text{(cells facing west or east)} \quad (11)$$
$$\eta_y = 0, \ \ if \ \ \hat{n} = \pm\hat{\jmath} \ \text{(cells facing north or south)}$$

In order to speed up computation, the idea is to exploit the linear approach. Since boundary cells are fixed, they can be consulted only once, then to store those cells to be used at each iteration, avoiding unnecessary *if-else* statements.

To do that, each cell information about the state of neighboring cells needs to be stored. We define these states as active or inactive, depending on whether the boundary condition must be applied or not.

The right neighbor cell information is a boolean array defined as

$$v^r_{p,q} = 1, \ \ if \ \ h_{p+1,q} < 0 \ (Land\ domain) \quad (12)$$
$$v^r_{p,q} = 0, \ \ if \ \ h_{p+1,q} \geq 0 \ (water\ domain)$$

and similarly, for $v^l_{p,q}$,$v^u_{p,q}$ and $v^d_{p,q}$.

Figure 1b illustrates boolean information for boundary conditions.

Recall that $v_{p,q}$ are arrays only dependent on the bathymetry data and do not change over time.

This allows to write a single boundary condition equation free of *if-else* statements

https://doi.org/10.5194/egusphere-2023-3061
Preprint. Discussion started: 22 January 2024

$$\eta_{p,q}^{k+1} = A_{p,q}\eta_{p,q}^{k} + \frac{1}{\left(1 + \frac{\alpha_{p,q}\Delta t}{2}\right)}\left(\zeta_{p,q}^{k+1} - 2\zeta_{p,q}^{k} + \zeta_{p,q}^{k-1}\right) + D_{p,q}\eta_{p,q}^{k-1} +$$

$$\left(1 - \nu_{p,q}^{r}\right)\left[B_{p,q}^{r} + \nu_{p,q}^{l}B_{p,q}^{l}\right]\eta_{p+1,q}^{k} + \left(1 - \nu_{p,q}^{l}\right)\left[B_{p,q}^{l} + \nu_{p,q}^{r}B_{p,q}^{r}\right]\eta_{p-1,q}^{k} +$$

$$\left(1 - \nu_{p,q}^{u}\right)\left[B_{p,q}^{u} + \nu_{p,q}^{d}B_{p,q}^{d}\right]\eta_{p,q+1}^{k} + \left(1 - \nu_{p,q}^{d}\right)\left[B_{p,q}^{d} + \nu_{p,q}^{u}B_{p,q}^{u}\right]\eta_{p,q-1}^{k} \quad (13)$$

2.4 Propagation in Spherical Coordinates

Strictly speaking, tsunamis occur over a spherical surface. The special case of transoceanic simulations requires incorporating the earth curvature. It is also possible to include other second order effects, such as Coriolis, nonetheless, for simplicity, we neglect it in this approach.

The original linear shallow water equation in spherical coordinates is

$$\eta_{tt} - \frac{g}{R_T^2 cos^2(\theta)}\left[(h\eta_\lambda)_\lambda + cos(\theta)(h\, cos(\theta)\eta_\theta)_\theta\right] = \zeta_{tt} \quad (14)$$

where $R_T = 6371\, km$, is the earth radius, λ is the longitude and θ is the latitude. Nevertheless, the equation discretization remains similar and the coefficients are

$$A_{i,j} = \frac{1}{\left(1 + \frac{\alpha_{i,j}\Delta t}{2}\right)}\left[2 - \frac{R}{cos^2(\theta_j)}\left(h_{i+\frac{1}{2},j} + h_{i-\frac{1}{2},j}\right) + \frac{cos\left(\theta_{j+\frac{1}{2}}\right)}{cos(\theta_j)}Rh_{i,j+\frac{1}{2}} + \frac{cos\left(\theta_{j-\frac{1}{2}}\right)}{cos(\theta_j)}Rh_{i,j-\frac{1}{2}}\right] \quad (15)$$

$$D_{i,j} = \frac{\alpha_{i,j}\Delta t - 2}{\alpha_{i,j}\Delta t + 2}$$

$$B_{i,j}^{r} = \frac{2Rh_{i+\frac{1}{2},j}}{cos^2(\theta_j)(2 + \alpha_{i,j}\Delta t)}$$

$$B_{i,j}^{l} = \frac{2Rh_{i-\frac{1}{2},j}}{cos^2(\theta_j)(2 + \alpha_{i,j}\Delta t)}$$

$$B_{i,j}^{d} = \frac{cos\left(\theta_{j-\frac{1}{2}}\right)}{cos(\theta_j)}\frac{2Rh_{i,j-\frac{1}{2}}}{2 + \alpha_{i,j}\Delta t}$$

$$B_{i,j}^{u} = \frac{cos\left(\theta_{j+\frac{1}{2}}\right)}{cos(\theta_j)}\frac{2Rh_{i,j+\frac{1}{2}}}{2 + \alpha_{i,j}\Delta t}$$

but in this case, $R = \left(\frac{\Delta t}{R_T \Delta s}\frac{180}{\pi}\right)^2$ and $\Delta s, \lambda, \theta$ are in degrees. Δs represents the space step in spherical coordinates.

2.5 Inhomogeneous Forcing Term

When external forces are “feeding” the shallow water equations, they have to be discretized accordingly with the numerical scheme.

https://doi.org/10.5194/egusphere-2023-3061
Preprint. Discussion started: 22 January 2024

In the case of tsunamigenic earthquakes, the minimum information required to compute the kinematic history of the seafloor disturbance is contained in the Finite Fault Model (FFM). When no time is involved, the initial condition can be simply computed with the Okada analytical solution (Okada, 1985). We call $\zeta_0(x,y)$ the static deformation of the seafloor.

If an earthquake is modeled with N_s subfaults, the static seafloor deformation is obtained simply by linear superposition

$$\zeta_0(x,y) = \sum_{n=1}^{N_s} \zeta_0^n(x,y) \quad (16)$$

Note that the summation order is irrelevant since we are aiming for the final status of the displacement. Instead, if we want to include temporal features, we need to employ the rise-time and rupture time. Rise time $t_R(x,y)$ accounts for duration of each sub fault and rupture time $t_V(x,y)$ indicates the activation time of a given subfault.

Each sub fault is simulated with a triangular source time rate function. The normalized fundamental integrated source time function is

$$\begin{aligned} S(\tau) &= 0, && if \quad \tau < 0 \\ S(\tau) &= 2\tau^2, && if \quad 0 \le \tau < 0.5 \\ S(\tau) &= 4\tau - 2\tau^2 - 1, && if \quad 0.5 \le \tau < 1 \\ S(\tau) &= 1, && if \quad 1 \le \tau \end{aligned} \quad (17)$$

Then, the kinematic seafloor deformation is computed as

$$\zeta(x,y,t) = \sum_{n=1}^{N_s} \zeta_0^n(x,y) S\left(\frac{t - t_v(x,y)}{t_R(x,y)}\right) \quad (18)$$

Computationally, Okada equations can be calculated in a parallel thread, but they have to be weighted and time-shifted according the function S.

The final displacement status can be incorporated into the bathymetry as a simple sum of the arrays, allowing the tsunami to propagate on the deformed state of the seafloor.

3 Algorithm Implementation

3.1 Computational and numerical considerations

When the seismic source solution is known, the water column perturbation is estimated using the seafloor deformation computed with the Okada equations. As mentioned before, the tsunami can be modeled using the described algorithm which can be implemented on any programming language. Particularly, for this study, the main routine was coded in a bash script that handles the execution and contains all the variables. The seafloor deformation from the seismic source and the tsunami solver were written in C, using parallel threads. Post-processing, reading, extraction and visualization were developed in Python.

To apply the model, the bathymetry must be known at some resolution. This is an important factor because it defines the amount of points on the grid and therefore, the computing time of the model. The implementation is determined by a combination of grid size and resolution, depending on how rapid and accurate one needs to issue a tsunami warning.

https://doi.org/10.5194/egusphere-2023-3061
Preprint. Discussion started: 22 January 2024

To optimize the pre-processing, we store 3 precomputed areas (see figure 2), extracted from the GEBCO global grid, with different resolutions; (a) including continental, oceanic islands and Antarctic Chilean territories (from 12°S to 68°S and 51°W to 115°W) with 15, 30, 45 and 60 arc seconds of resolution, (b) only continental and near continent oceanic islands (from 17.5°S to 57°S and 67°W to 82°W) with 30 arc seconds of resolution and (c) a Pacific basin area (), which is crop from a global grid (from 70°N to 70°S and 180°E to 180°W) with 60, 120 and 180 arc seconds resolution. The area (a) is meant to be used for any earthquake in the Chilean near field, meaning that a megathrust earthquake in the subduction zone, an outer rise earthquake between Easter Island and the continental territory, an earthquake in front of Peru, or one in the Antarctic Peninsula can be assessed. The area (b) is selected mainly for subduction earthquakes in front of the Chilean continental territory, but can also be used for any other mechanism within the area like at outer rise in the subducting plate before the subduction zone, and can provide a threat asset for the continental land and the nearest islands (Juan Fernandez and San Felix). The (c) area can be used for any earthquake within the Pacific basin (e.g. Japan trench, Aleutian subduction zone, Hikurangi subduction zone), but the global grid can take an event almost anywhere, leaving the north and south poles out for numerical reasons. In terms of spatial variables, this model allows to define in a simple manner the extension of the geographic domain. For example, one of the pre-computed grids can be trimmed to a specific area before the computation, which gives versatility to the amount of points in the grid. This is implemented with four variables that determine the geographical extension using as initial limits the borders of the fault plane and adding a given distance to the north, south, east and west as input parameters.

https://doi.org/10.5194/egusphere-2023-3061
Preprint. Discussion started: 22 January 2024

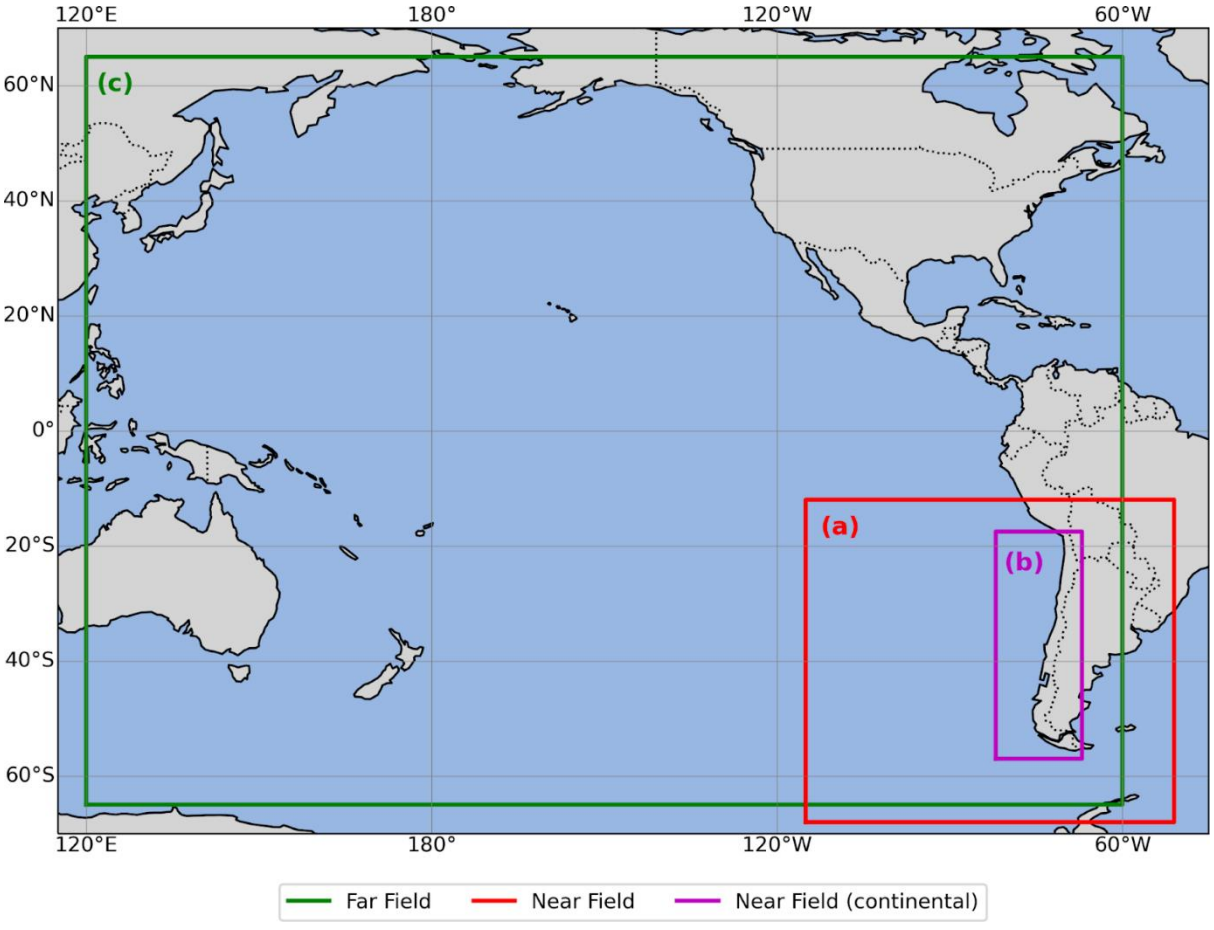

Figure 2: Pre-computed grid extensions. (a) Near field grid extension including all Chilean territories (i.e. continental, oceanic islands and Antarctic). (b) Near field grid extension including only continental and near continental islands. (c) Far field grid extension considering the Pacific basin as the tsunami threat generation zone for Chile.

When the spatial resolution and geographical extension of the domain are set, time steps are determined using the CFL condition, which is necessary to ensure numerical stability of the solver. Considering that CFL < 1, Δt is conditioned by

$$\Delta t_{max} < \frac{R_T \Delta \cos(|\theta_{max}| - \Delta s/2)}{\sqrt{2gh_{max}}}, \quad (19)$$

Figure 3 shows the result of the tsunami propagation model for the Maule (Chile) 2010 earthquake, whose seismic source is available at the USGS Earthquake Catalog website, using an extension that was calculated adding to the fault plane limits, 4° to the north and south, 0.5° to the west and 0.1° to the east. The simulation takes a spatial resolution of 30'', Δt = 1.0 s and a total simulation time of 5 hours.

https://doi.org/10.5194/egusphere-2023-3061
Preprint. Discussion started: 22 January 2024

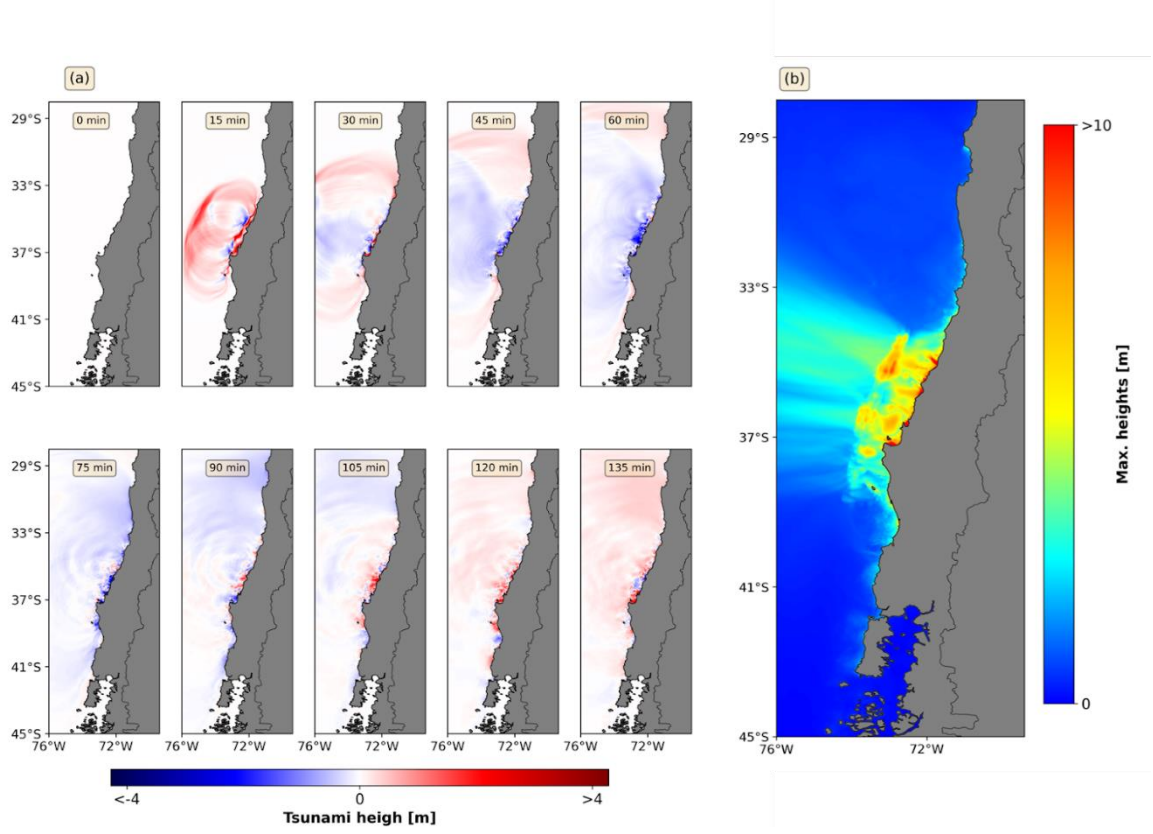

Figure 3: Example of a tsunami modelling using the described algorithm for the Maule 2010 (Chile) earthquake, with 5 hours of simulation time. (a) Snapshots of the water surface. (b) Maximum amplitude distribution.

Two types of seismic solutions are implemented; a point source from which an elliptical finite fault model is created and a finite fault model determined directly from the seismic data (GPS, broadband seismometers and accelerometers). Both are shown in figure 4. At first, only the point source is available and after a few minutes the FFM is expected to be computed and ready to be used. To validate the model only finite fault solutions were used, as they accurately represent the physics of the earthquake.

https://doi.org/10.5194/egusphere-2023-3061
Preprint. Discussion started: 22 January 2024

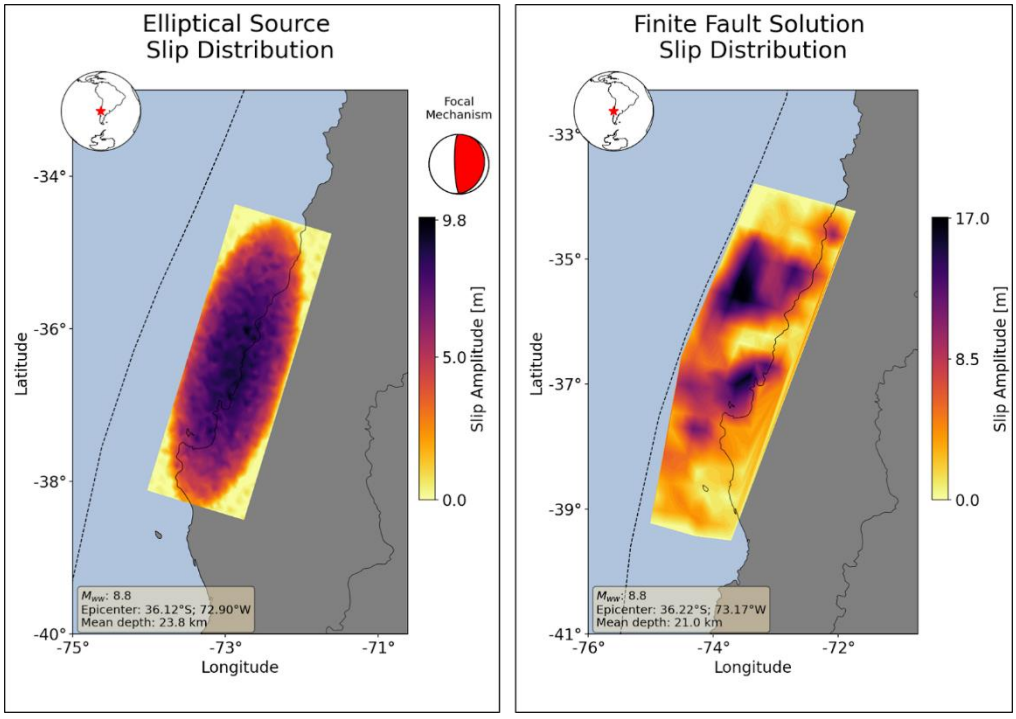

Figure 4: Finite fault models of the Maule (2010) earthquake. On the left, an elliptic source slip distribution model generated from the point source solution. On the right, the finite fault model published by the USGS (USGS, 2022).

3.2 Model Validation

This model considers the generation and propagation phases of a tsunami and therefore can be compared to tsunami observations in sea level gauges and buoys. The model was validated with the observations available of several tsunamis that were registered in Chile.

Figure 5 shows a comparison between the registered Maule (2010), Tohoku-Oki (2011), Pisagua (2014), Illapel (2015) and Melinka (2016), using the finite fault solutions for the earthquake as input in our numerical solver. Some stations that correctly recorded the tsunami waves are chosen to compare and validate the model.

https://doi.org/10.5194/egusphere-2023-3061
Preprint. Discussion started: 22 January 2024

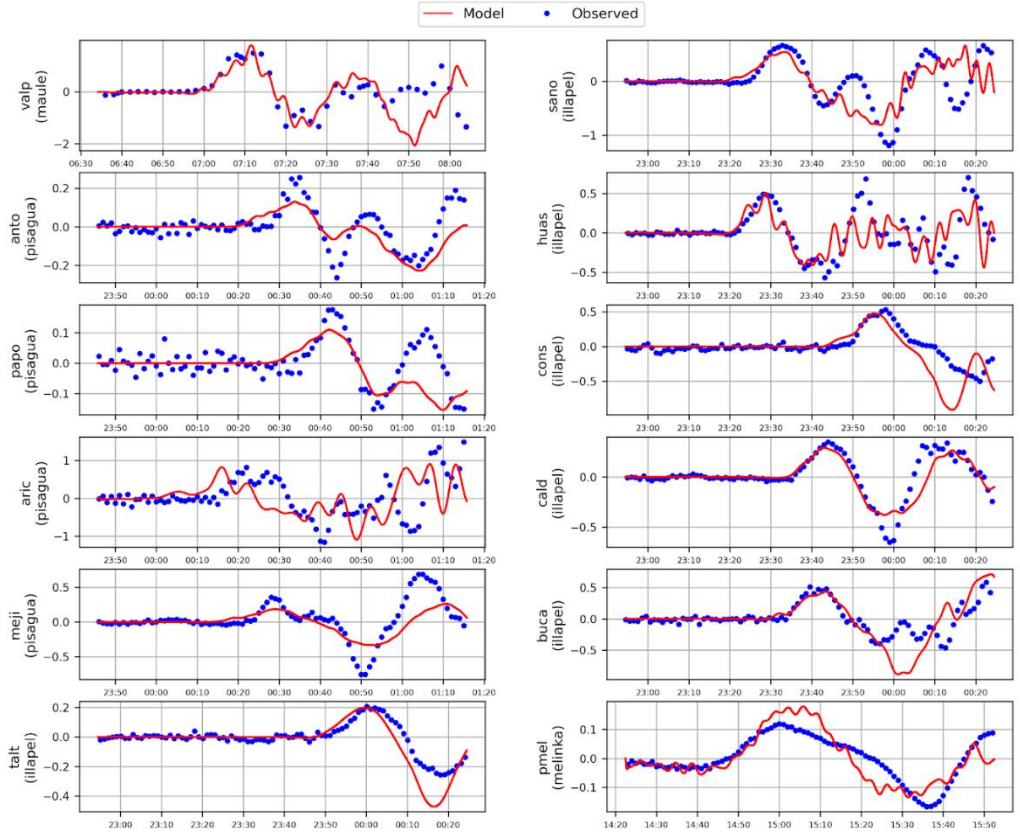

Figure 5: Comparison between tsunami observed on sea level stations and modelled using FFM for the Maule 2010, Pisagua 2014, Illapel 2015 and Melinka 2016 events.

It can be observed that there is an accurate agreement between the first arrivals (considering time, polarity and amplitude), for the stations near the source. As the distance from the generation zone increases, more differences start to appear. This behavior can be explained mainly by 2 reasons. The first is directly related to the mathematical approach being used, as the higher order terms of the equations are dismissed and therefore some physics of the tsunami propagation is lost. The second one is associated with the discretization of the domain. This can lead to a loss of characteristics of the coastal shape which can be relevant. For example, some bays may lose some of their geometry leading to a loss of a resonance phenomenon that should be incorporated. The largest difference in arrival times for local tsunami sources in front of the Chilean coast was less than 10 minutes.

https://doi.org/10.5194/egusphere-2023-3061
Preprint. Discussion started: 22 January 2024

3.3 Studied Cases

To test the model, recent earthquakes that generated a tsunami threat for Chilean coasts were used. The source parameters were extracted from the final source solution published in the USGS earthquake catalogue website, for the Tocopilla 2007, Maule 2010, Tohoku-Oki 2011, Pisagua 2014 (main shock and its aftershock), Illapel 2015 and Melinka 2016. Note that all of them were in the near field (off the coast of Chile), except the Japan 2011 earthquake.

The figure 6 shows a surface projection representation of the slip distribution from the finite fault models extracted from the USGS earthquake catalogue, for each event. To model the tsunami, different parameters were used, obtaining tsunami threat evaluations according to them. Figure 7 shows the resulting threat evaluation for each case considering the near field case (domain from Fig. 2 (a)). Figures 7 (a)-(f), are evaluated after 12 hours of simulations, while figure 7 (f) shows the tsunami threat evaluation for a far field event (domain from Fig. 2 (c)), after 24 hours of simulation.

https://doi.org/10.5194/egusphere-2023-3061
Preprint. Discussion started: 22 January 2024

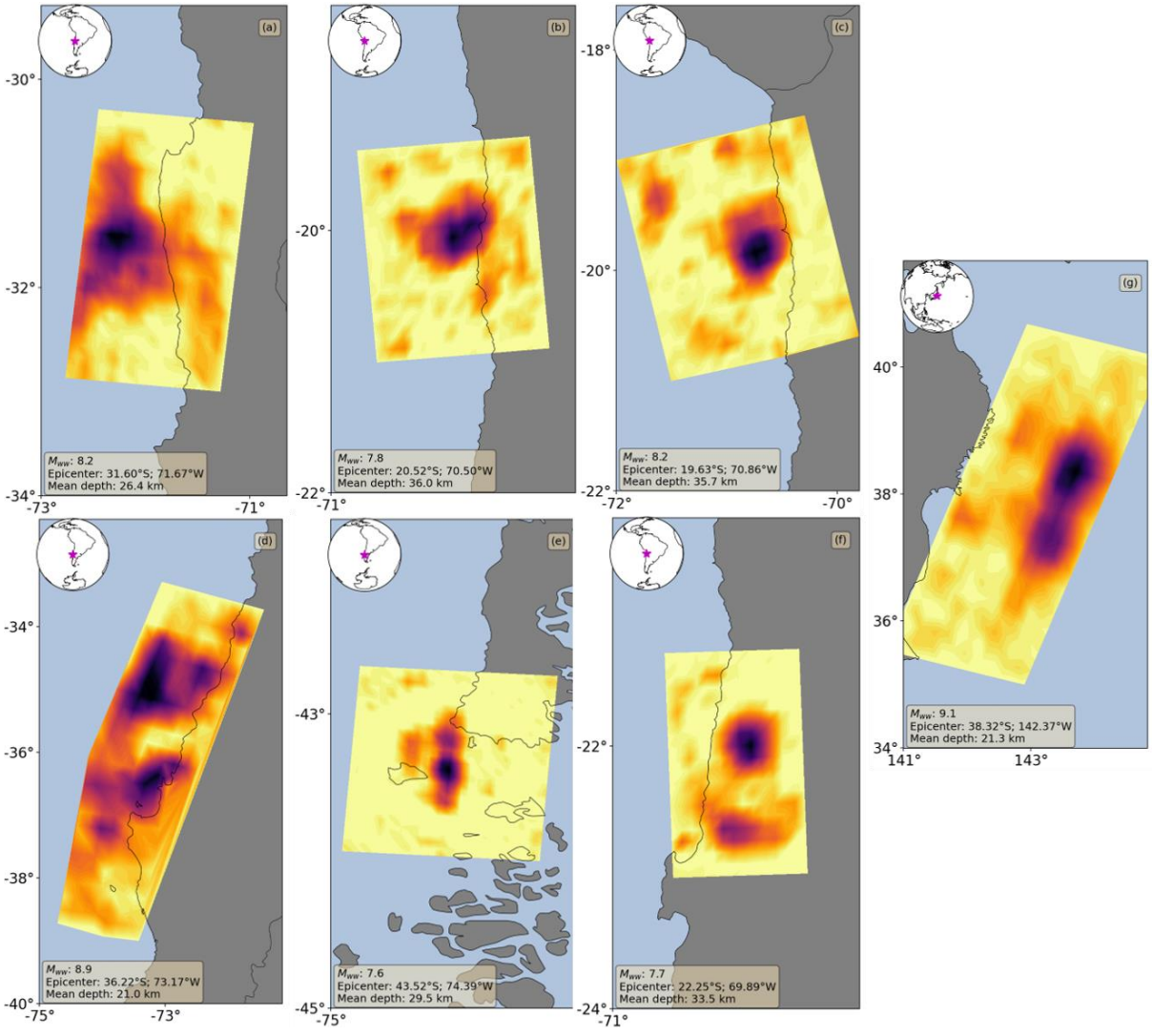

Figure 6: Representation of the projection of the slip distribution on the surface of the earthquakes used to test the model, using the USGS earthquake catalogue finite fault models. The earthquakes shown are (a) Illapel 2015, (b) Pisagua 2014, (c) Pisagua 2014, (d) Maule 2010, (e) Melinka 2016, (f) Tocopilla 2007 and (g) Tohoku-Oki 2011.

https://doi.org/10.5194/egusphere-2023-3061
Preprint. Discussion started: 22 January 2024

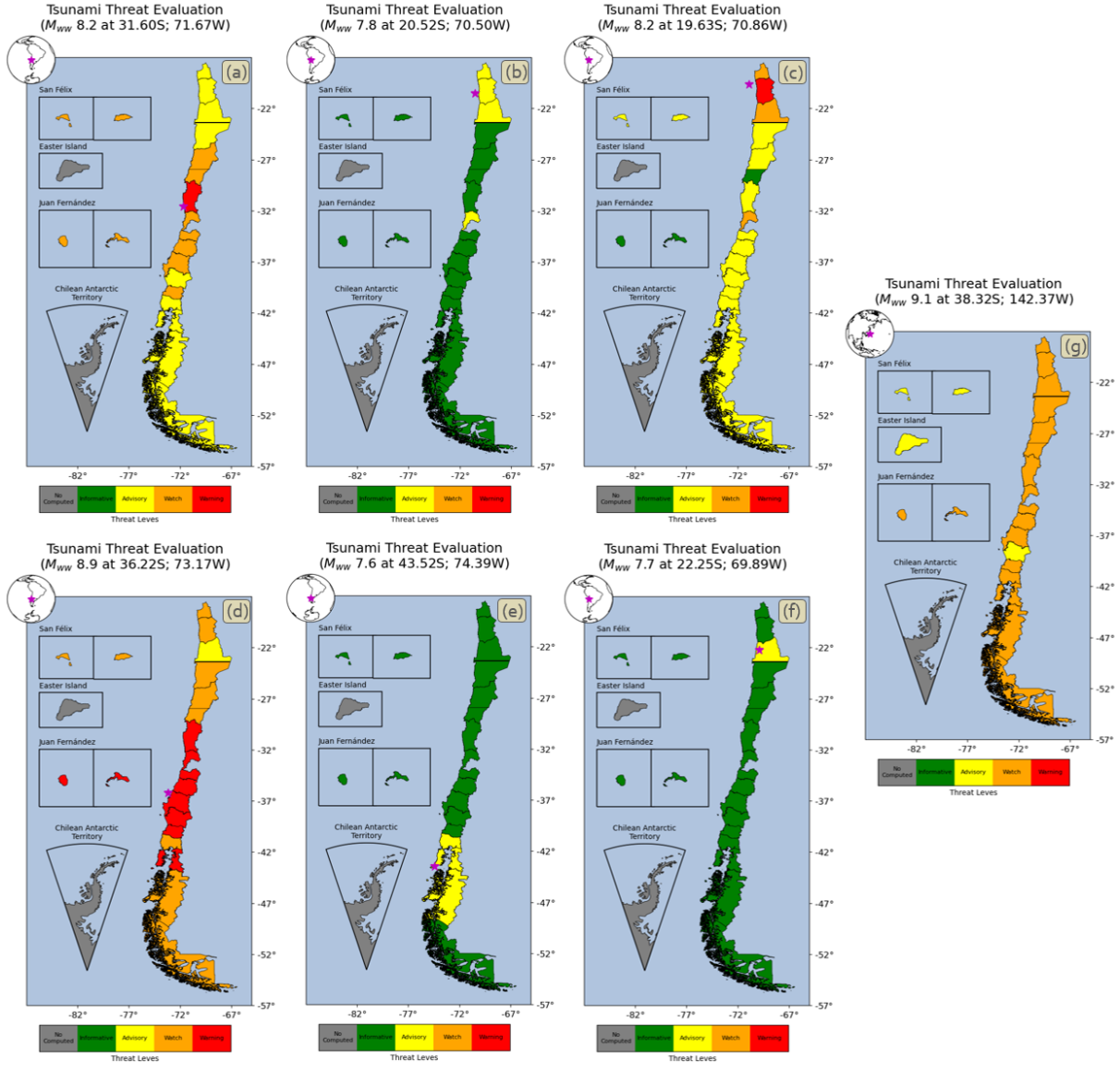

255 **Figure 7: Tsunami threat evaluations obtained as a result of modelling the tsunami generated by the sources shown in figure 6, corresponding to (a) Illapel 2015, (b) Pisagua 2014, (c) Pisagua 2014, (d) Maule 2010, (e) Melinka 2016, (f) Tocopilla 2007 and (g) Tohoku-Oki 2011.**

4 Early Warning Application

260 ### 4.1 Tsunami Threat Evaluation

To apply this methodology into an operational framework for early warning purposes, first, the data used to plot the results shown in figure 3 are transformed into a tsunami threat product.

https://doi.org/10.5194/egusphere-2023-3061
Preprint. Discussion started: 22 January 2024

The Chilean territory is divided into 21 geographical blocks, already implemented by the Chilean National Tsunami Warning System. Each block is assigned with one of the four defined threat levels: Informative, Advisory, Watch and Warning (Catalán et al. 2020, ONEMI, SHOA & FCFM, 2019). An extra level is included, named "Not computed". The simulation time can vary, leaving some blocks without a tsunami threat because they might be out of the domain or the tsunami wave has not yet arrived to a given block.

Also, the same thresholds were used to determine the threat levels for each block, defined in table 1.

Table 1: Threat levels defined on the Chilean Tsunami Early Warning System (ONEMI, SHOA & FCFM, 2019).

Threat Level	Expected coastal tsunami height (H)	Associated colour
Informative	$H < 0.3$ [m]	Green
Advisory	$0.3 \leq H < 1.0$ [m]	Yellow
Watch	$1.0 \leq H < 3.0$ [m]	Orange
Warning	$H \geq 3.0$ [m]	Red

In order to calculate the threat level for each block, several points were created separated by 10 km along the coast. Each point belongs to only one block. However, they are manually placed considering the morphology of the coast. Also, the current sea level gauges in the Chilean coast, oceanic islands and the Antarctic Peninsula were included, obtaining more than 640 points (see Figure 8a). The maximum tsunami height is analyzed to determine the tsunami threat of each block, being enough that at least one point on that block exceeds the threshold value to be classified on the higher level.

https://doi.org/10.5194/egusphere-2023-3061
Preprint. Discussion started: 22 January 2024

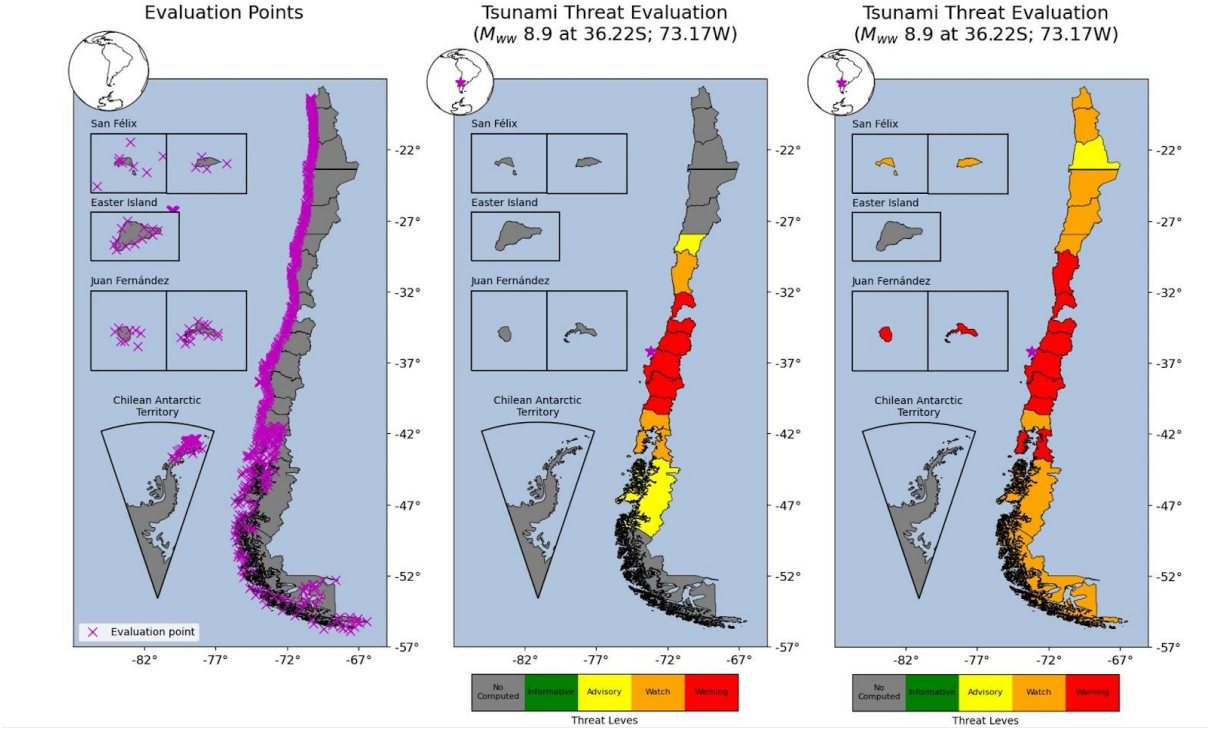

Figure 8: (a) Tsunami threat evaluation points for Chile and the 21 blocks division. (b) Tsunami threat for Chile using the Maule 2010 earthquake as tsunami source, with a restricted spatial domain and 5 hours of simulation. (c) Same seismic source as (b) but with a restricted spatial domain and 5 hours of simulation. (c) Same seismic source as (b) but with 12 hours of simulation and spatially restricted to continental and oceanic islands near the continent blocks.

The results from the tsunami model are used to assess a tsunami threat for Chile using the maximum coastal tsunami heights at the evaluation points shown in Figure 8 (a), resulting in threat levels in Figure 8 (b). The tsunami threat is obtained using an heterogeneous seismic source considering its rupture time, with a regular spatial resolution of 30 arc seconds in a restricted domain, with time step of 1 second and a total simulation time of 5 hours; the computation time to obtain this threat map is of 117 seconds, while the result in figure 8 (c) took about 12.5 minutes. The differences between figures 8 (b) and (c) are the simulation time (from 5 to 12 hours) and the spatial domain. The election of the parameters that led to these results with the mentioned computation times are not random and the reasons are explained forward.

4.2 Early Warning Validation

4.2.1 Threat Asset

The time between the tsunami generation and the issuing of threat messages is crucial. This is the reason why we neglect the higher order terms of the equations and reduce the spatial resolution of the domain, as long as these features do not heavily modify the tsunami behaviour.

https://doi.org/10.5194/egusphere-2023-3061
Preprint. Discussion started: 22 January 2024

Then, it remains only to choose the set of parameters that have a threat asset in the required time. The time threshold chosen is (according to the actual Chilean Early Tsunami Warning System Protocol) 5 minutes after the reception of the seismic source information.

A performance test was designed to match the mix of parameters that accomplish the required time. The computation time will depend on the amount of points in the spatial domain, the total simulation time, the time step and the computational environment in which the program is executed. The maximum time step that will allow numerical stability is given by the CFL condition, which will lead to only 2 parameters to be modified; points in the grid and total simulation time. The second is direct to implement, considering that enough simulation time is needed for the tsunami to reach most of the geographical extent, thus, the best combination between extent and resolution need to be found. The resolution is expected to be such that it does not lead to spatial changes that could significantly modify the tsunami propagation. The geographical extent should be enough to warn communities about an imminent tsunami. After the first bulletin, there is more time to extend the evaluation (timely and geographically), since the communities closer to the generation source were already informed.

The four parameters used to generate the performance tests were the spatial resolution, the geographical extent in both latitude and longitude and the total simulation time. Time step was calculated as the 80% of the maximum value according to the CFL condition. The numerical domain is chosen as the minimum rectangle that encloses the finite fault.Then extended as detailed in Table 2. Notice that the longitudinal extension keeps fixed 0.5° to the East, because the Chilean coast is located always to the east side of the source. To the west, the values are chosen including islands while in the latitudinal cases, the same distance is considered for both North and South. Each combination was run 3 times to check the stability on computation time and the run was repeated if the standard deviation was higher than a 10% of the computation time.

Table 2: Values for each parameter to be varied in the performance test. The extensions take into account the sign, as usual, and they are measured from the limits of the fault plane.

Parameter	Values
Spatial resolution	15; 30; 45 arc seconds
Latitudinal extension	[-1°,1°]; [-2°,2°]; [-4°,4°]; [-6°,6°]; [-8°,8°];
Longitudinal extension	[-0.5°, 0.5°]; [-6°, 0.5°]; [-8°, 0.5°]

The tests were executed in a server with 2 processors, 18 cores with a total of 72 sub processes, a basic frequency of 3,1 GHz and maximum turbo frequency of 4,00 GHz. The compilers were Intel OneAPI (icc, icpc, ifort) and GNU version 8.5.0 (gcc, g++, gfortran).

The results of the performance test showed that many combinations allowed results in less than 2 minutes proving that it would be useful for tsunami early warning.

https://doi.org/10.5194/egusphere-2023-3061
Preprint. Discussion started: 22 January 2024

4.2.2 Tsunami Travel Times (TTT)

When tsunami travel time calculation is included, the total computation time increases no more than 5 seconds. The precision of the arrival times depends on the spatial resolution and the distance from the source. The arrival times are calculated for each point on the grid that has a real station associated. A comparison was made between the arrival times computed with the model and the registered arrival times from the 2010, 2014 and 2015 events, obtaining less than 10 minutes of difference in each station.

Special considerations are needed for the fjords and inland waters. The geographical area given by the spatial resolution may incorrectly represent some waterways, making the tsunami travel through a different path (i.e. longer path) increasing the travel time calculated.

5 Discussion of the Proposed Procedure

While there is no finite fault solution, we model the tsunami using the fault plane defined by the W-phase moment tensor. Once the FFM is available, it triggers a subsequent simulation.

Early warning aims to give the authorities the information needed to take actions before disasters happen, in this particular case, before the tsunami impacts on the coast. This means to define the threat level timely for each block and not necessarily all at once.

To improve the performance for early warning and diminish the possibility of human mistakes during the evaluation process, 4 predefined versions of parameter combinations are proposed to achieve different objectives, for an earthquake in the subduction zone between Nazca and South American plates.

The first version is thought to be the fastest and uses a point source as input, which results in a threat assessment for the coastal communities closer than ~ 250 [km], in North-South directions, of the epicentre with 3 hours of simulation time. This version of the evaluation takes less than 50 seconds to compute. The second version can either use a point source or if available, a FFM that produces an evaluation for the coast closer than ~ 750 [km], in North-South directions, from the source with 4 hours of simulation time. The third version includes all continental regions to be evaluated and therefore the computation time is higher (~ 10 [min]). The first time this version is run, it should be with the same spatial resolution of the previous versions but with 12 hours of simulation time.

Chilean territory in the other continents such as Easter Island and The Antarctic are treated separately. Given the extension of the bathymetry, we execute two instances of tsunami modelling one that includes only the continental territory (figure 2, b) and the other that cover the continental and insular territory, and the Antarctic (figure 2, a). This ensures to have a first tsunami warning map for the continental territory in ~ 12.5 minutes.

For the far field case, there is more time to react. Therefore, we use a fixed set of parameters to model the tsunami in the Pacific region, with a bathymetry of 2’ arc resolution and at 24 hours of tsunami simulation time. This case takes ~ 20 minutes to compute.

https://doi.org/10.5194/egusphere-2023-3061
Preprint. Discussion started: 22 January 2024

The proposed time frame is shown in figure 9, considering the time lapses in which source solutions with the necessary parameters can be obtained, according to Riquelme et al (2021). The parameters of each solution are detailed and the optimal parameters and conditions for each evaluation for both, near and far field scenarios. Note that in the last near field evaluation, two spatial resolutions are shown, where the only difference with the previous case is that Easter Island and Antarctica are included, leading into an large increasing in the tsunami domain extension (see figure 2); the optimal case is to maintain the same spatial resolution through the whole process, since a degradation of the spatial resolution may lead to a decrease on the threat level for some blocks because of the loss of details of the geomorphology but, depending mainly on the source location, there may not be enough time to compute the evaluation using the same resolution to obtain threat levels for Easter Island and Antarctica, so a lower spatial resolution can result into a good approach in useful times to decide if an evacuation is necessary or not for those two territories, while keeping the threat levels for the rest of the blocks from the previous evaluation. If this is the case, after obtaining the evaluation with a lower resolution, a new evaluation should be computed using its previous value. For the far field scenario, given the larger reaction time, it's affordable to wait for the FFM source solution to be computed. Finally, there is always the possibility to include manually all the parameters, to shape the outcome for particular cases.

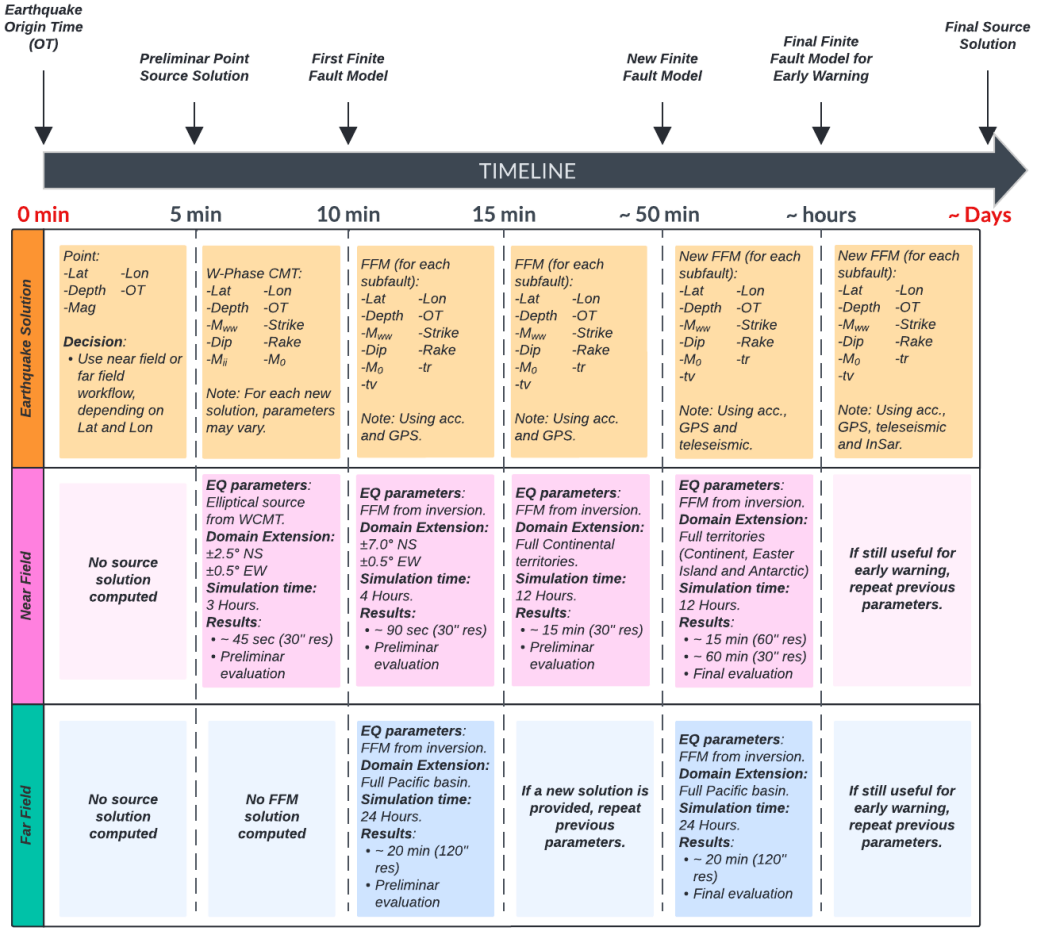

https://doi.org/10.5194/egusphere-2023-3061
Preprint. Discussion started: 22 January 2024

Figure 9: Time frame for the implementation of the model for tsunami early warning, considering a near field and far field scenario, for the predefined versions. For a far field case, there is no need to evaluate the threat with a point source solution, given the reaction time to evacuate if necessary. The earthquake solution times and parameters were extracted from Riquelme et al. (2021).

6 Conclusions

The strategy presented can be implemented on a Tsunami Early Warning System. The seismic source solution obtained by the Chilean National Seismological Center, with the W-Phase method, is used as the first input to compute the tsunami threat levels for Chile within less than 10 minutes, through a numerical tsunami propagation model.

The optimization of the boundary condition allows to reduce computation time via a linear approach of the first order terms of the shallow water equations and a fixed coastal boundary condition.

The versatility in the extent and resolution of the grid, allows a flexible amount of points in the grid handled by the user, resulting in a model that can obtain the tsunami threat levels for the necessary communities depending on the reaction time.

This methodology uses a heterogeneous finite fault that considers all the known heterogeneities (up to that time) of the earthquake, diminishing the biases imposed by other strategies, as the precomputed scenarios.

The predefined versions of the code allow to choose alternatives such as point source or finite fault model, near or far field earthquakes. Therefore, there is a customized model for each alternative. This benefits the affected communities relying on the reaction time, decreases the level of complexity, diminishes the computation time and reduces the probabilities of human errors in a stressed context of operation.

Competing interests

The contact author has declared that none of the authors has any competing interest.

Acknowledgments

This work was partially funded by Progama de Riesgo Sísmico (PRS) and Fondecyt grant 1211105. The authors also thanks to the Servicio Hidrográfico y Oceanográfico de la Armada (SHOA), for supporting the master thesis of Matias Sifón.

References

Aránguiz,R.,González,G.,González,J.,Catalán,P.A.,Cienfuegos,R.,Yagi,Y.,... Rojas, C. (2015). The 16 September 2015 Chile Tsunami from the Post-Tsunami Survey and Numerical Modeling Perspectives. Pure and Applied Geophysics, 173(2), 333–348. doi:10.1007/s00024-015-1225-4

https://doi.org/10.5194/egusphere-2023-3061
Preprint. Discussion started: 22 January 2024

Barrientos, S., y Ward, S. (1990). The 1960 Chile earthquake: inversion for slip distribution from surface deformation. Geophysical Journal International, 103(3), 589–598. doi:10 .1111/j.1365-246X.1990.tb05673.x

Catalán,P.,Aránguiz,R.,González,G.,Tomita,T.,Cienfuegos,R.,González,J.,... Gubler, A. (2015). The 1 April 2014 Pisagua tsunami:Observations and modeling. Geophysical Research Letters, 42(8), 2918–2925. doi:10.1002/2015GL063333

Catalan, P. A., Gubler, A., Cañas, J., Zuñiga, C., Zelaya, C., Pizarro, L., Valdes, C., Mena, R., Toledo, E., and Cienfuegos, R. (2020). Design and operational implementation of the integrated tsunami forecast and warning system in Chile (SIPAT). Coastal Engineering Journal, 62(3), 373 - 388. https://doi.org/10.1080/21664250.2020.1727402

Fritz, H., Petroff, C., Catalán, P., Cienfuegos, R., Winckler, P., Kalligeris, N., ... Synolakis, C. (2011). Field survey of the 27 february 2010 chile tsunami. Pure and Applied Geophysics, 168, 1989-2010. doi:10.1007/S00024-011-0283-5

Fuentes, M., Riquelme, S., Hayes, G., Medina, M., Melgar, D., Vargas, G., Gonzalez, G., and Villalobos, A. (2017). A study of the 2015 Mw 8.3 Illapel earthquake and tsunami: Numerical and analytical approaches. Pure and Applied Geophysics. 173, 1847 - 1858.

Fuentes, M., Arriola, S., Riquelme, S., and Delouis, B. (2019). Speeding up tsunami forecasting to boost tsunami warning in Chile. Natural Hazards and Earth System Sciences, 19(6), 1297-1304.

Geist, E. L. (2002). Complex earthquake rupture and local tsunamis. Journal of Geophysical Research: Solid Earth, 107(B5), ESE-2.

United Nations Educational, Scientific and Cultural Organization, Intergovernmental Oceanographic Commission. UNESCO/IOC (2017). Manuals and Guides 76. Plans and Procedures for Tsunami Warning and Emergency Management.

Lomnitz, C. (2004). Major Earthquakes of Chile: A Historical Survey, 1535-1960. Seismological Research Letters, 75, 368–378.

Madariaga, R. (1998). Sismicidad de Chile. Física de La Tierra, 10, 221–258.

ONEMI, SHOA y FCFM. (2019). Protocolo Oficina Nacional de Emergencia del Ministerio del Interior y Seguridad Pública, Servicio Hidrográfico y Oceanográfico de la Armada y Centro Sismológico Nacional de la Facultad de Ciencias Físicas y Matemáticas de la Universidad de Chile para Eventos de Sismo y Tsunami en las Costas de Chile. Santiago, Chile.

Okada, Y. (1985). Surface deformation due to shear and tensile faults in a half-space. Bulletin of the seismological society of America, 75(4), 1135-1154.

Riquelme, S., Koch, P., Goldberg, D., Melgar, D., & Yeck, W. (2021). Expansion of the NEIC finite fault modeling capabilities to include regional seismic and geodetic data. In AGU Fall Meeting 2021, held in New Orleans, LA, 13-17 December 2021, id. S55F-0208.

Riquelme, S., and Fuentes, M. (2021). Tsunami efficiency due to very slow earthquakes. Seismological Society of America, 92(5), 2998-3006.

Ruiz, J., Fuentes, M., Riquelme, S., Campos, J., and Cisternas, A. (2015) Numerical simulation of tsunami runup in northern Chile based on non-uniform k−2 slip distributions. Natural Hazards 79, 1177-1198.

Stein, S., and Michael, W. (2003). An introduction to seismology, earthquakes, and Earth structure. Blackwell Publishing.

https://doi.org/10.5194/egusphere-2023-3061
Preprint. Discussion started: 22 January 2024

Kanamori, H. (1977). The energy release in great earthquakes. Journal of Geophysical Research, 82(20). doi: https://doi.org/10.1029/JB082i020p02981

United States Geological Service (USGS). (2022). Earthquake Hazards Program. https://earthquake.usgs.gov/earthquakes/eventpage/official20100227063411530_30/finite-fault?source=us&code=usp000h7rf.